



Speed-sensorless predictive torque control of the IM based on MRAS ASM'nin MUS tabanlı hız-algılayıcısız öngörülü moment kontrolü

Rıdvan Demir^{1,*} , Recep Yıldız² , Murat Barut³ 

¹ Kayseri University, Electrical Electronic Engineering Department, 38280, Kayseri, Türkiye

^{2,3} Niğde Ömer Halisdemir University, Electrical Electronic Engineering Department, 51240, Niğde, Türkiye

Abstract

In this study, an induction motor (IM) drive based on speed-sensorless predictive torque control (PTC) is designed to perform the high-performance control of the IMs by utilizing the least mean square (LMS) algorithm for the adaptation mechanism of the model reference adaptive system (MRAS). Here, the MRAS with LMS adaptation is based on the stator currents ($i_{s\alpha}$ and $i_{s\beta}$) of the IM. Moreover, the rotor fluxes ($\varphi_{r\alpha}$ and $\varphi_{r\beta}$) are obtained by the current model, which requires the rotor mechanical speed (ω_m) along with $i_{s\alpha}$ and $i_{s\beta}$. In contrast to the other MRAS based studies using proportional-integral (PI) in the adaptation mechanisms to estimate state or parameter, it is possible to determine the states and/or parameters as weight coefficients in the MRAS with LMS adaptation which are calculated and updated in each iteration. Here, ω_m value is estimated and updated in each iteration as weight coefficient. Furthermore, the MRAS with LMS adaptation is compared to the MRAS using conventional PI in simulations. The simulation results clearly visualize both the estimation performance of stator current based MRAS using LMS adaptation and the effectiveness of the proposed PTC based IM drive.

Keywords: Speed-sensorless IM control, PTC, LMS algorithm, MRAS

1 Introduction

Due to the devastating effects of climate change, CO₂ emissions have attracted the attention of people all over the world. Thus, instead of using fossil fuels in vehicles, the electrical vehicles have been becoming more and more popular these days, which points out the importance of electrical motors and their control strategies. Induction motor (IM) is one of the used electric motors in electrical vehicles and industry. Some of the reasons for the use of IMs can be given as low maintenance requirement, cost, simplicity, and ability to work in harsh environments. Considering the high performance control applications of the IMs, different methods are used in the current literature such as field oriented control (FOC) [1], direct torque control (DTC) [2, 3], and model predictive control (MPC) [4, 5]. In the literature, there are some studies emphasizing the superiorities of the FOC over the DTC or vice versa [6, 7]. Here, MPC is rather new comparing to the other methods in the IM control applications. In the literature, one of the most

Öz

Bu çalışmada, asenkron motorların (ASM'lerin) yüksek başarılı kontrolünü gerçekleştirmek için uyarlama mekanizmasında en küçük ortalama kareler (EKOK) algoritmasını kullanan modele uyarlamalı sisteme (MUS'a) dayanan hız-algılayıcısız öngörülü moment kontrol (ÖMK) tabanlı ASM sürücüsü tasarlanmıştır. Burada, EKOK uyarlamalı MUS ASM'nin stator akımları ($i_{s\alpha}$ ve $i_{s\beta}$) tabanlıdır. Rotor akıları ($\varphi_{r\alpha}$ ve $\varphi_{r\beta}$), rotor mekanik hızı (ω_m) ile birlikte $i_{s\alpha}$ ve $i_{s\beta}$ gerektiren akım model kullanılarak elde edilmiştir. Uyarlama mekanizmasında oransal-integral kullanan MUS tabanlı çalışmaların aksine, EKOK uyarlamalı MUS'da durum ve/veya parametreler her iterasyonda hesaplanan ve güncellenen ağırlık katsayıları olarak tanımlanabilir. Bu çalışmada ω_m her iterasyonda ağırlık katsayısı olarak kestirilir ve güncellenir. Ayrıca, EKOK uyarlamalı MUS geleneksel oransal-integrali kullanan MUS ile benzetim ortamında karşılaştırılmıştır. Benzetim sonuçları EKOK uyarlamalı kullanılan stator akımları tabanlı MUS'un kestirim başarımını ve önerilen ÖMK tabanlı ASM sürücüsünün etkinliğini açıkça göstermektedir.

Anahtar kelimeler: Hız-algılayıcısız ASM kontrolü, MÖK, EKOK algoritması, MUS

preferred MPC strategies for the control of IMs is the predictive torque control (PTC) [8]. In the PTC strategy, the electromagnetic torque and stator flux are controlled by the proper selection of the voltage vector, which determines the inverter switching states [9]. By determining the proper voltage vector, the reference flux and electromagnetic torque values are tracked by PTC [9]. By the minimization of the cost function, which is defined by the control objectives in PTC, the optimal voltage vector is selected. Here in PTC, new control constraints and objectives can be added to the cost function [4]. Although there is no need for inner current control loops, there is only one PI controller for the outer speed control loop in PTC [8]. As addressed by Rodriguez et al. [4], by considering the computational optimization, the parameter sensitivity, the weight factor adjustment, and the switching frequency limitation, more efficient PTC strategies can be developed. Thus, there are some studies for the enhancement of PTC strategies by reducing switching frequency [9], minimizing power loss [10], optimizing or

* Sorumlu yazar / Corresponding author, e-posta / e-mail: ridvandemir@kayseri.edu.tr (R. Demir)

Geliş / Received: 22.11.2022 Kabul / Accepted: 26.12.2022 Yayınlanma / Published: 15.01.2023

doi: 10.28948/ngumuh.1208031

eliminating weight factor [11, 12], and increasing robustness against the parameter variations [13].

Along with the advantages of the IMs, their highly nonlinear models and parameter variations make the high performance control applications challenging. Here, the parameter variations address the frequency and temperature based resistance variations and flux level based inductance variations. Control performance of the IM drives is related to the correct values of the states and thus parameters. In order to obtain the correct values of the control objectives, model based methods are used in the literature such as model reference adaptive system (MRAS) [14], full order observers [15], sliding mode observer (SMO) [16], and nonlinear Kalman filters [17].

Considering these methods, MRAS based methods stand especially out due to simplicity and computational load when considering a simple microprocessor application. Looking at the MRAS based studies in the literature, Schauder [18] presents rotor mechanical speed (ω_m) estimation by using the voltage and current model of the IM in the reference and adaptive model of the flux based MRAS, respectively. Vasic et al. [19] use the flux based MRAS for parallel estimation of the stator resistance (R_s) and ω_m . In Gayathri et al. [20], the rotor resistance (R_r) estimation is performed by using the rotor flux based MRAS. In Mapelli et al. [21], the reactive power and motor torque based two different MRAS algorithms are implemented and compared. Demir and Barut [22] present an active power based MRAS algorithm using the least mean square (LMS) method in the adaptation mechanism to estimate R_s along with the other estimated states and parameters by an extended Kalman filter. Teja et al. [23] introduce an X based MRAS for R_s estimation when ω_m is measured. In Teja et al. [23], X represents a stator voltage and current based fictitious quantity. In Basak et al. [24], an active power and Y based MRAS algorithm is performed for R_s estimation, and X based MRAS algorithm is used for the ω_m estimation. As X in Teja et al. [23], Y represents a fictitious quantity in [24]. Orłowska-Kowalska and Dybkowski [25] present a MRAS algorithm based on stator current to estimate ω_m . In Bednarz and Dybkowski [14], a MRAS algorithm based on reactive and active power is performed to estimate R_s and R_r . The rotor time constant (T_r) is estimated by MRAS using least square method [1].

The main contribution of this study is to perform the speed-sensorless PTC based IM drive by using the stator currents based MRAS. Here, the LMS is utilized in the adaptation mechanism of the MRAS to perform ω_m estimation. The estimated ω_m is fed back to both PTC and the current model of the IM used to obtain the rotor fluxes ($\varphi_{r\alpha}$ and $\varphi_{r\beta}$). $\varphi_{r\alpha}$ and $\varphi_{r\beta}$ are used in both PTC to obtain stationary axis components of stator fluxes ($\varphi_{s\alpha}$ and $\varphi_{s\beta}$) and adaptive model to obtain stator currents ($i_{s\alpha}$ and $i_{s\beta}$). Instead of using the proportional-integral (PI) controller adaptation in MRAS, the LMS algorithm provides the opportunity to determine states and/or parameters as weight coefficient to calculate and update in each iteration, which can be classified as another contribution of this study. By using LMS adaptation in MRAS, the PI controller need for the conventional MRAS is eliminated. Therefore, there is no

need to design PI controller and determine its coefficients, which is a time consuming process. Furthermore, in order to show the effectiveness of the MRAS with LMS adaptation, it is compared with the MRAS using conventional PI in the same scenario in simulations. The comparison results are presented both graphically and numerically.

This paper is composed of six sections. The related literature review and contribution of this study is given in Section I. The dynamic model of the IMs is given in Section II. The details of the stator current based MRAS algorithm and LMS adaptation based speed estimation are presented in Section III. Section IV and Section V present the details of proposed PTC based IM drive and the simulation results, respectively. Finally, the conclusion is clarified in Section VI.

2 Dynamic model of the IM

The dynamic model of the IM based on rotor flux can be divided into two subsystems: the electrical and mechanical. The electrical subsystem can be described by fourth-order mathematical equations as follows:

$$\frac{di_{s\alpha}}{dt} = -\left(\frac{R_s}{L_\sigma} + \frac{R_r L_m^2}{L_r^2 L_\sigma}\right) i_{s\alpha} + \frac{L_m R_r}{L_r^2 L_\sigma} \varphi_{r\alpha} \quad (1)$$

$$\frac{di_{s\beta}}{dt} = -\left(\frac{R_s}{L_\sigma} + \frac{R_r L_m^2}{L_r^2 L_\sigma}\right) i_{s\beta} - \frac{L_m p_p \omega_m}{L_\sigma L_r} \varphi_{r\alpha} \quad (2)$$

$$\frac{d\varphi_{r\alpha}}{dt} = \frac{R_r L_m}{L_r} i_{s\alpha} - \frac{R_r}{L_r} \varphi_{r\alpha} - p_p \omega_m \varphi_{r\beta} \quad (3)$$

$$\frac{d\varphi_{r\beta}}{dt} = \frac{R_r L_m}{L_r} i_{s\beta} + p_p \omega_m \varphi_{r\alpha} - \frac{R_r}{L_r} \varphi_{r\beta} \quad (4)$$

As for the mechanical subsystem, it is defined by a mathematical equation derived from the equation of motion as follows:

$$\frac{d\omega_m}{dt} = \frac{3 p_p L_m}{2 J_T L_r} (\varphi_{r\alpha} i_{s\beta} - \varphi_{r\beta} i_{s\alpha}) - \frac{B_T}{J_T} \omega_m - \frac{t_L}{J_T} \quad (5)$$

where $\alpha\beta$ – represents stator stationary axis; $v_{s\alpha}$, $v_{s\beta}$, $i_{s\alpha}$, and $i_{s\beta}$ are the $\alpha\beta$ – axis components for stator voltages and currents; $\varphi_{r\alpha}$ and $\varphi_{r\beta}$ are the $\alpha\beta$ – axis components for rotor fluxes; ω_m is rotor mechanical speed; R_r and R_s are rotor and stator resistances, respectively; L_r and L_s are rotor and stator leakage inductances, respectively; L_m is magnetizing inductance; $L_\sigma = \sigma L_s = L_s - L_m^2/L_r$ is stator transient inductance; p_p is number of pole pairs; J_T and B_T are the total inertia of system and viscous friction coefficient, respectively [26].

In this study, so as to perform the estimation of $i_{s\alpha}$, $i_{s\beta}$, $\varphi_{r\alpha}$, $\varphi_{r\beta}$, and ω_m , the electrical subsystem equations given in Equation (1)-(4) are used in the MRAS algorithm. Here, (3) and (4) represent the current model of the IM.

3 Stator current based MRAS

The flowchart for the conventional stator current based

MRAS algorithm using PI controller and MRAS algorithm using LMS adaptation are shown in Figure 1 [25] and Figure 2. In this MRAS estimators, while the measured $i_{s\alpha}$ and $i_{s\beta}$ are outputs of the reference model, the adaptive model outputs are obtained by Equations (6) and (7). $\varphi_{r\alpha}$ and $\varphi_{r\beta}$ required for Equations (6) and (7) are provided by Equations (8) and (9), which are the current model. Here, Equations (6)-(9) are obtained by discretizing Equations (1)-(4) with forward Euler approximation.

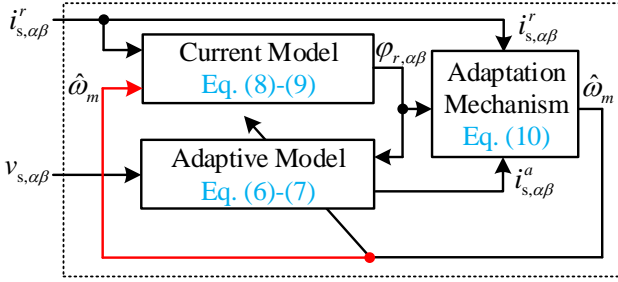


Figure 1. The stator current based MRAS using conventional PI [25].

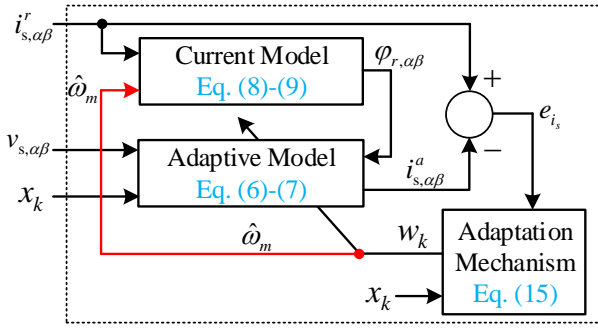


Figure 2. The stator current based MRAS with LMS adaptation

$$i_{s\alpha,k+1}^a = \left(1 - T \left(\frac{R_s}{L_\sigma} + \frac{R_r L_m^2}{L_r^2 L_\sigma}\right)\right) i_{s\alpha,k} + \frac{T}{L_\sigma} v_{s\alpha,k} + \frac{L_m R_r T}{L_r^2 L_\sigma} \varphi_{r\alpha,k} + \frac{L_m p_p \omega_{m,k} T}{L_\sigma L_r} \varphi_{r\beta,k} \quad (6)$$

$$i_{s\beta,k+1}^a = \left(1 - T \left(\frac{R_s}{L_\sigma} + \frac{R_r L_m^2}{L_r^2 L_\sigma}\right)\right) i_{s\beta,k} + \frac{T}{L_\sigma} v_{s\beta,k} - \frac{L_m p_p \omega_{m,k} T}{L_\sigma L_r} \varphi_{r\alpha,k} + \frac{L_m R_r T}{L_r^2 L_\sigma} \varphi_{r\beta,k} \quad (7)$$

$$\varphi_{r\alpha,k+1} = \frac{R_r L_m T}{L_r} i_{s\alpha,k} + \left(1 - \frac{R_r T}{L_r}\right) \varphi_{r\alpha,k} - T p_p \omega_{m,k} \varphi_{r\beta,k} \quad (8)$$

$$\varphi_{r\beta,k+1} = \frac{R_r L_m T}{L_r} i_{s\beta,k} + T p_p \omega_{m,k} \varphi_{r\alpha,k} + \left(1 - \frac{R_r T}{L_r}\right) \varphi_{r\beta,k} \quad (9)$$

In order to perform speed estimation in MRAS algorithm using conventional PI adaptation, Equations (6)-(9) and measured stator currents are used in Equation (10).

$$\omega_m^{PI} = \left(k_p + \frac{k_i}{s}\right) \left((i_{s\alpha}^r - i_{s\alpha}^a) \varphi_{r\beta} - (i_{s\beta}^r - i_{s\beta}^a) \varphi_{r\alpha}\right) \quad (10)$$

For the MRAS estimator with LMS adaptation, the weight vector (\mathbf{w}_k) and the input matrix (\mathbf{x}_k) of the adaptive model given in Equations (6) and (7) are defined as follows:

$$\mathbf{w}_k = \begin{bmatrix} 1 - T \left(\frac{R_s}{L_\sigma} + \frac{R_r L_m^2}{L_r^2 L_\sigma}\right) \\ \frac{L_m R_r T}{L_r^2 L_\sigma} \\ \frac{T L_m p_p \omega_{m,k}}{L_\sigma L_r} \\ \frac{T}{L_\sigma} \end{bmatrix} \quad (11)$$

$$\mathbf{x}_k = \begin{bmatrix} i_{s\alpha,k} & i_{s\beta,k} \\ \varphi_{r\alpha,k} & \varphi_{r\beta,k} \\ \varphi_{r\beta,k} & \varphi_{r\alpha,k} \\ v_{s\alpha,k} & v_{s\beta,k} \end{bmatrix} \quad (12)$$

where other coefficients except for ω_m in \mathbf{w}_k are constant. Using Equations (11) and (12), the adaptive model outputs can be rewritten as follows:

$$\begin{bmatrix} i_{s\alpha,k+1}^a \\ i_{s\beta,k+1}^a \\ i_{s,k}^a \end{bmatrix} = \mathbf{x}_k^T \mathbf{w}_k \quad (13)$$

The difference between the reference model outputs (measured $i_{s\alpha}$ and $i_{s\beta}$) and the adaptive model outputs, namely errors, are defined by Equation (14).

$$\mathbf{e}_{i_s,k} = \mathbf{i}_{s,k}^r - \mathbf{i}_{s,k}^a \quad (14)$$

In the LMS algorithm, \mathbf{w}_k is updated by using the $\mathbf{e}_{i_s,k}$ and \mathbf{x}_k according to Equation (15).

$$\mathbf{w}_{k+1} = \mathbf{w}_k + \mu \mathbf{x}_k \mathbf{e}_{i_s,k} \quad (15)$$

where μ is called the step size controlling stability and the convergence rate of the LMS algorithm. So as to guarantee the stability of the LMS algorithm, μ must theoretically be selected as in Equation (16) [22, 27].

$$0 < \mu < 2/\lambda_{max} \quad (16)$$

In Equation (16), λ_{max} represents the greatest eigenvalue of the correlation matrix $\mathbf{R} = \mathbf{E}\{\mathbf{x}_k \mathbf{x}_k^T\}$ [27].

4 PTC based IM drive

In this paper, to perform the speed-sensorless control of the IM, the PTC drive system is chosen due to its advantages.

As can be seen from the IM drive block diagram in Figure 3, $i_{s\alpha}$, $i_{s\beta}$, $\varphi_{r\alpha}$, $\varphi_{r\beta}$ and ω_m are required for the PTC algorithm. The required $i_{s\alpha}$, $i_{s\beta}$, and ω_m values are obtained by using the stator current based MRAS structure, which utilizes the current model of the IM to perform $\varphi_{r\alpha}$ and $\varphi_{r\beta}$ estimations. By estimating $\varphi_{r\alpha}$ and $\varphi_{r\beta}$ with the help of the current model, the estimated $\varphi_{s\alpha}$ and $\varphi_{s\beta}$ are obtained for the PTC algorithm as in Equation (19) [8].

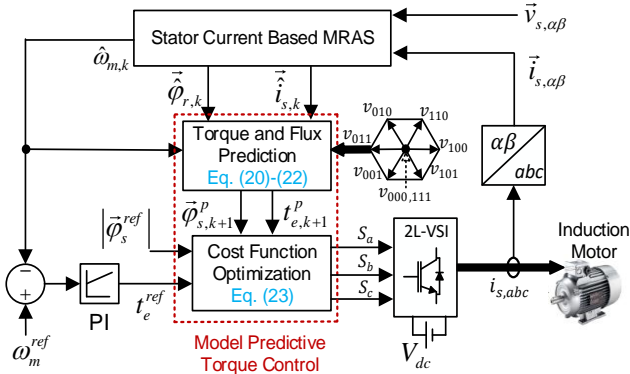


Figure 3. MRAS based speed-sensorless IM drive based on PTC

In the IM drive, the inverter is the two-level voltage source inverter (2L-VSI). The eight inverter switching vectors are also presented in Figure 3. Furthermore, the 2L-VSI voltage source inverter topology and the switching vectors are presented in Figure 4. In Figure 4, S_a , S_b , and S_c are the switching states associated with each phase, and V_{dc} represents the DC link voltage of the inverter. Moreover, if $S_x = 1$, S_x represents the ON state and \bar{S}_x represents the OFF state, $S_x \in \{S_a, S_b, S_c\}$ [13]. Here, the inverter switching state (\vec{S}) and the inverter output voltage (\vec{v}_s) are presented in Equations (17) and (18), respectively:

$$\vec{S} = \frac{2}{3}(S_a + \bar{a}S_b + \bar{a}^2S_c) \quad (17)$$

$$\vec{v}_s = V_{dc}\vec{S} \quad (18)$$

where $\bar{a} \triangleq e^{j2\pi/3}$ and V_{dc} represents the inverter DC link voltage as in Figure 3.

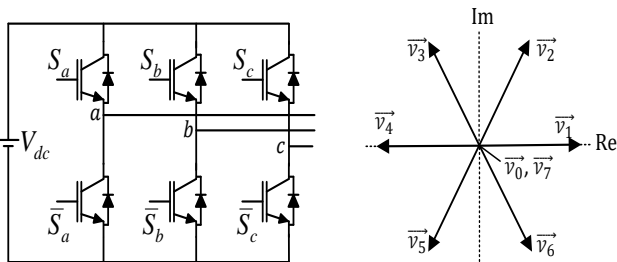


Figure 4. 2L-VSI topology and the possible eight voltage vectors.

In order to obtain the estimated stator flux vector ($\vec{\varphi}_{s,k}$) required for the PTC, the estimated stator current vector ($\vec{i}_{s,k}$) and the estimated rotor flux vector ($\vec{\varphi}_{r,k}$) are used in each iteration. $\vec{\varphi}_{s,k}$ is obtained as in Equation (19) [4, 8, 28].

$$\vec{\varphi}_{s,k} = \frac{L_m}{L_r} \vec{\varphi}_{r,k} + L_\sigma \vec{i}_{s,k} \quad (19)$$

In order to perform the PTC algorithm, the predicted stator voltage vector ($\vec{\varphi}_{s,k+1}^p$), the predicted stator current vector ($\vec{i}_{s,k+1}^p$), and the predicted electromagnetic torque vector ($t_{e,k+1}^p$) are required. For this purpose, $\vec{\varphi}_{s,k+1}^p$ value at the time $k+1$ is obtained by using the voltage model of the IM for each voltage vector as in Equation (20). The expressions for the $\vec{i}_{s,k+1}^p$ and $t_{e,k+1}^p$ are given in Equations (21) and (22) at the time $k+1$ [8, 28, 29].

$$\vec{\varphi}_{s,k+1}^{p(j)} = \vec{\varphi}_{s,k} + T(\vec{v}_{s,k}^{p(j)} - R_s \vec{i}_{s,k}), j \in \{0, 1, \dots, 7\} \quad (20)$$

$$\vec{i}_{s,k+1}^{p(j)} = \frac{T}{T+T_\sigma} \left(\frac{1}{R_\sigma} \left(\frac{k_r}{T_r} - k_r j \hat{\omega}_r \right) \vec{\varphi}_{r,k} + \vec{v}_{s,k}^{p(j)} \right) + \left(1 + \frac{T}{T_\sigma} \right) \vec{i}_{s,k}, j \in \{0, 1, \dots, 7\} \quad (21)$$

$$t_{e,k+1}^{p(j)} = \frac{3}{2} p_p \Im \{ (\vec{i}_{s,k+1}^{p(j)}) (\vec{\varphi}_{s,k+1}^{p(j)})^* \}, j \in \{0, 1, \dots, 7\} \quad (22)$$

where $T_\sigma = L_\sigma/R_\sigma$, $T_r = L_r/R_r$, $R_\sigma = R_s + k_r^2 R_r$, $\hat{\omega}_r = p_p \hat{\omega}_m$, and $k_r = L_m/L_r$.

The presented predicted values ($\vec{\varphi}_{s,k+1}^{p(j)}$ and $t_{e,k+1}^{p(j)}$) are used in a predefined cost function. In order to obtain the optimal switching vectors, predicted values calculated for all switching vector are applied to cost function. Therefore, the voltage vector minimizing the cost function given in Equation (23) is chosen as optimal switching vector.

$$g = \sum_{h=1}^N \left\{ \left| t_e^* - t_{e,k+h}^{p(j)} \right| + \gamma \left| |\vec{\varphi}_s^*| - |\vec{\varphi}_{s,k+h}^{p(j)}| \right| + I_{m,k+h} \right\} \quad (23)$$

Here in Equation (23), γ is the weighting factor determining the relative effect of the stator flux on the cost function, N is the prediction horizon ($N = 1$ in this paper), I_m refers to the overcurrent protection, which is given in Equation (24) [4, 8, 28].

$$I_{m,k+h} = \begin{cases} 0, & \text{if } |\vec{i}_{s,k+1}^p| \leq i_{s,max} \\ \infty, & \text{if } |\vec{i}_{s,k+1}^p| > i_{s,max} \end{cases} \quad (24)$$

5 Simulations

In order to test the robustness and performance of the proposed speed-sensorless drive in simulations, the block diagram given in Figure 3 is designed and implemented in Matlab/Simulink. As stated before, a PI controller whose

coefficient is chosen by using trial-and-error method is used in the outer speed control loop of the IM drive. A three phase squirrel-cage IM, whose rated parameters and values are presented in Table 1, is used in Figure 3. In simulations; sampling time (T) is determined as $25\mu s$; weighting factor (γ) in cost function is determined as 50; step size (μ) of the LMS algorithm is chosen as 0.5.

Table 1. Rated values and parameters for IM used in simulations.

P [kW]	V [V]	I [A]	f [Hz]
3	380	6.9	50
n_{mn} [r/min]	t_L [N.m]	p_p	R_s [Ω]
1430	20	2	2.283
R_r [Ω]	L_s [H]	L_r [H]	L_m [H]
2.133	0.2311	0.2311	0.22

In simulation studies, a scenario including rated speed for both directions of operation, low speed operation, and zero speed operation of the IM is designed. Moreover, t_L applied to the IM is changed both in linear and step-like manner to examine the robustness of the proposed IM drive against different types of t_L changes. The applied stator flux amplitude reference ($|\varphi_s|^{ref}$), the rotor mechanical speed reference (n_m^{ref}) for the IM drive, and the applied t_L for IM are presented in Figure 5 for the challenging scenario.

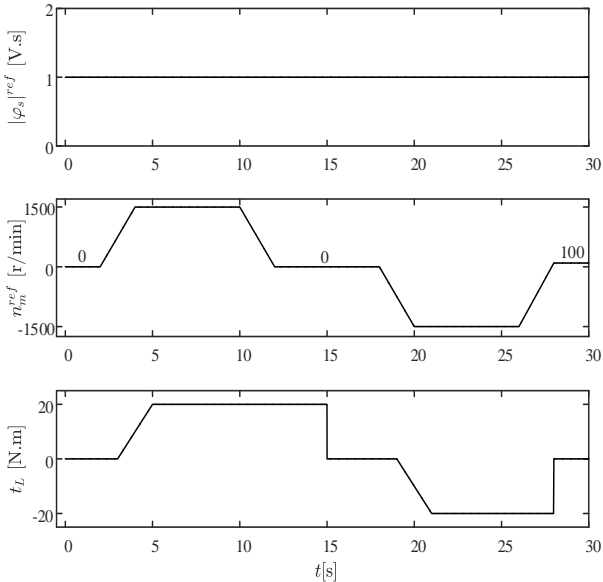


Figure 5. The applied $|\varphi_s|^{ref}$ and n_m^{ref} values for the IM drive together with the applied t_L to the IM.

The estimation results obtained by stator current based MRAS with LMS adaptation and the control performance for the proposed speed-sensorless PTC based IM drive is presented in Figure 6. The associating estimation errors of the MRAS with LMS adaptation are given in Figure 7. Here

in Figures 6 and 7, the measured values are represented by “ \cdot^m ”, the estimated values are represented by “ $\hat{\cdot}$ ”, and associating estimation errors determined by the difference between the estimated and measured values are represented by “ $e_{(\cdot)}$ ”.

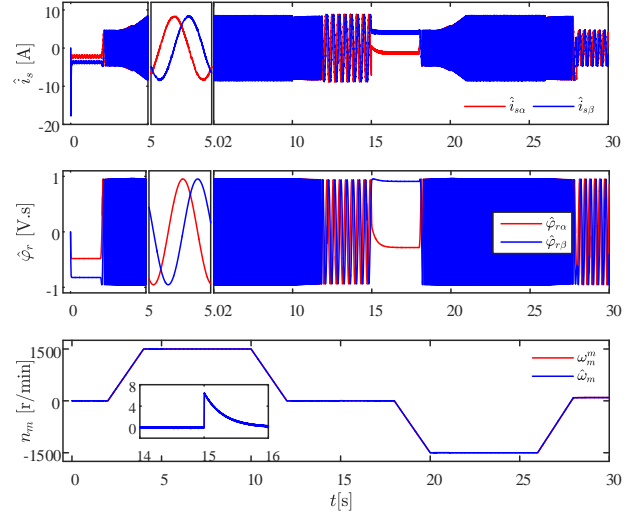


Figure 6. Corresponding estimations results for MRAS with LMS adaptation and the tracking results for the proposed IM drive.

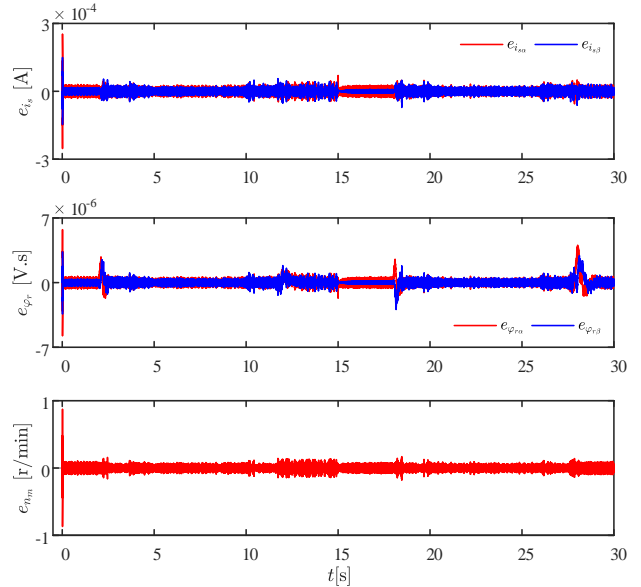


Figure 7. Estimation errors for the MRAS with LMS adaptation.

In order to show the performance of the proposed IM drive, the MRAS with LMS adaptation is compared to the MRAS using traditional PI adaptation for the scenario given in Figure 5. The estimation results and errors associating with MRAS using PI adaptation are presented in Figures 8 and 9, respectively.

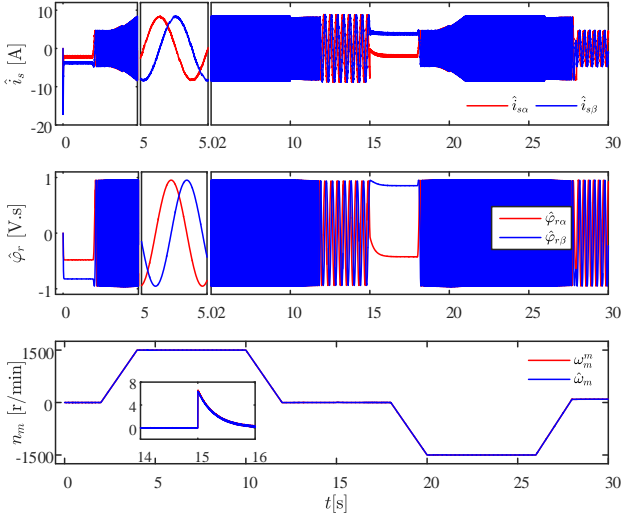


Figure 8. Corresponding estimations results for MRAS using conventional PI adaptation and the tracking results for the IM drive.

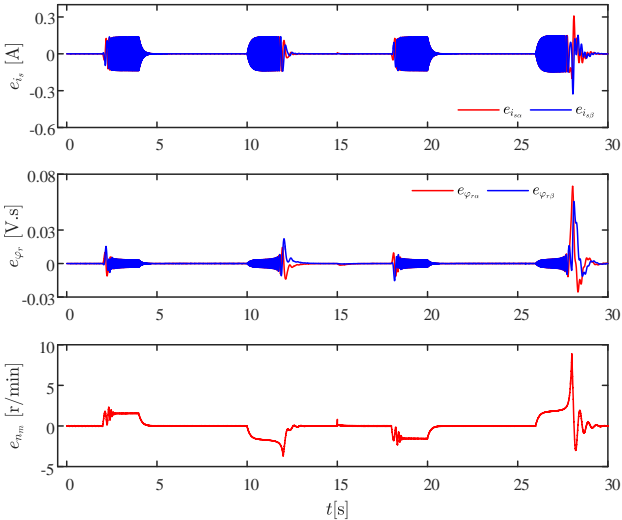


Figure 9. Estimation errors for the MRAS using conventional PI adaptation.

In the performance tests given in Figures 5-9, the high performance control of the IM is executed for a wide speed range with t_L changes. Considering the simulation results in Figures 6-9 for the proposed IM drive, the following detailed remarks can be deduced.

- Considering the comparison results given in Figures 6-9 for MRAS with LMS adaptation and MRAS using conventional PI, it can be seen that the MRAS estimator using LMS adaptation presents better estimation performance compared to the MRAS using conventional PI. This can be verified by considering the estimation errors presented in Figures 7 and 9.
- Although the proposed PTC based IM drive is tested under a wide speed range operation scenario, highly promising control and estimation performances are achieved for the proposed PTC based IM drive and MRAS with LMS adaptation.

- The zero speed and zero load torque condition called DC condition is tested in the scenario. It is clear from the Figures 6 and 7 that the proposed PTC based IM drive easily handles this challenging condition.
- As can be seen from Figure 5, there are linear and step-like t_L changes in the performance test. Due to the high estimation and control performance of the proposed PTC based IM drive system, it can be expressed that the proposed drive is robust against t_L variations as in Figures 6 and 7.

In order to demonstrate the comparison results of MRAS estimators numerically, the mean square errors (MSEs) related to the MRAS estimations are presented in Tables 2 and 3 for MRAS with LMS and MRAS using conventional PI, respectively.

Table 2. MSEs related to the estimations for MRAS with LMS adaptation (for Figure 7).

$e_{i_{s\alpha}}$ [A]	$e_{i_{s\beta}}$ [A]	$e_{\varphi_{r\alpha}}$ [V.s]	$e_{\varphi_{r\beta}}$ [V.s]
8.640×10^{-11}	5.463×10^{-11}	1.535×10^{-13}	1.013×10^{-13}
e_{n_m} [r/min]			
9.980×10^{-4}			

Table 3. MSEs related to the estimations for MRAS with conventional PI adaptation (for Figure 9).

$e_{i_{s\alpha}}$ [A]	$e_{i_{s\beta}}$ [A]	$e_{\varphi_{r\alpha}}$ [V.s]	$e_{\varphi_{r\beta}}$ [V.s]
2.760×10^{-3}	2.688×10^{-3}	2.787×10^{-5}	2.341×10^{-5}
e_{n_m} [r/min]			
1.084			

The presented MSE values in Tables 2 and 3 for MRAS estimators verify that the MRAS with LMS adaptation has better estimation performance than the MRAS using conventional PI. In this study, the step size for the MRAS with LMS adaptation and PI coefficients for conventional MRAS are determined by the trial-and-error method, and these values are crucial for the performance of the MRAS estimators. Therefore, it can be noted that a fair comparison results can be obtained by determining the optimal step size value and PI coefficient values by using metaheuristic optimization techniques.

6 Conclusion

In this paper, IM drive based on PTC is designed and tested for the speed-sensorless high performance control applications of the IMs. So as to perform the speed-sensorless PTC of IM, the stator current based MRAS with LMS adaptation is used. In the MRAS structure, $\varphi_{r\alpha}$ and $\varphi_{r\beta}$ is obtained by using the current model of the IM, which requires the rotor mechanical speed (ω_m) along with the $i_{s\alpha}$ and $i_{s\beta}$. Instead of using PI controller based adaptation mechanism in the stator current based MRAS, LMS based adaptation mechanism is used to perform the estimations in this paper. By using the LMS algorithm in adaptation mechanism, it is possible to determine ω_m as a weight coefficient in the LMS based MRAS algorithm which is

calculated and updated in each iteration. In order to test the proposed IM drive in simulations, a scenario including wide speed range operation of the IM with linear and step-like t_L variations is performed. The simulation results show robustness and effectiveness of the proposed IM drive. Moreover, the MRAS with LMS adaptation is compared with the MRAS using conventional PI. The presented results and MSE values show the superiority of the MRAS with LMS adaptation compared to the MRAS using conventional PI.

Conflict of interest

The authors declare that there is no conflict of interest.

Similarity rate (iThenticate): 19%

References

- [1] B. Reddy, G. Poddar, and B. P. Muni, 'Parameter Estimation and Online Adaptation of Rotor Time Constant for Induction Motor Drive', *IEEE Trans. Ind. Appl.*, 58(2), 1416–1428, 2022. <https://doi.org/10.1109/TIA.2022.3141700>.
- [2] I. M. Alsofyani and N. R. N. Idris, 'Simple Flux Regulation for Improving State Estimation at Very Low and Zero Speed of a Speed Sensorless Direct Torque Control of an Induction Motor', *IEEE Trans. Power Electron.*, 31(4), 3027–3035, 2016. <https://doi.org/10.1109/TPEL.2015.2447731>.
- [3] M. A. Usta, H. I. Okumus, and H. Kahveci, 'A simplified three-level SVM-DTC induction motor drive with speed and stator resistance estimation based on extended Kalman filter', *Electr. Eng.*, 99(2), 707–720, 2017. <https://doi.org/10.1007/s00202-016-0442-x>.
- [4] J. Rodriguez, R. M. Kennel, J. R. Espinoza, M. Trincado, C. A. Silva, and C. A. Rojas, 'High-Performance Control Strategies for Electrical Drives: An Experimental Assessment', *IEEE Trans. Ind. Electron.*, 59(2), 812–820, 2012. <https://doi.org/10.1109/TIE.2011.2158778>.
- [5] K. Wróbel, P. Serkies, and K. Szabat, 'Model Predictive Base Direct Speed Control of Induction Motor Drive—Continuous and Finite Set Approaches', *Energies*, 13(5), 1193, 2020. <https://doi.org/10.3390/en13051193>.
- [6] D. Casadei, F. Profumo, G. Serra, and A. Tani, 'FOC and DTC: two viable schemes for induction motors torque control', *IEEE Trans. Power Electron.*, 17(5), 779–787, 2002. <https://doi.org/10.1109/TPEL.2002.802183>.
- [7] F. Korkmaz, I. Topaloglu, H. Mamur, M. Ari, and I. Tarimer, 'Reduction of torque ripple in induction motor by artificial neural multinetworks', *Turk. J. Electr. Eng. Comput. Sci.*, 24, 3492–3502, 2016. <https://doi.org/10.3906/elk-1406-54>.
- [8] E. Zerdali and R. Demir, 'Speed-sensorless predictive torque controlled induction motor drive with feed-forward control of load torque for electric vehicle applications', *Turk. J. Electr. Eng. Comput. Sci.*, 29, 223–240, 2021. <https://doi.org/10.3906/elk-2005-75>.
- [9] K. V Praveen Kumar and T. V. Kumar, 'Enhanced direct torque control and predictive torque control strategies of an open-End winding induction motor drive to eliminate common-mode voltage and weighting factors', *IET Power Electron.*, 12(8), 1986–1997, 2019. <https://doi.org/10.1049/iet-pel.2018.5599>.
- [10] S. R. Eftekhari, S. A. Davari, P. Naderi, C. Garcia, and J. Rodriguez, 'Robust Loss Minimization for Predictive Direct Torque and Flux Control of an Induction Motor With Electrical Circuit Model', *IEEE Trans. Power Electron.*, 35(5), 5417–5426, 2020. <https://doi.org/10.1109/TPEL.2019.2944190>.
- [11] P. R. U. Guazzelli, W. C. de Andrade Pereira, C. M. R. de Oliveira, A. G. de Castro, and M. L. de Aguiar, 'Weighting Factors Optimization of Predictive Torque Control of Induction Motor by Multiobjective Genetic Algorithm', *IEEE Trans. Power Electron.*, 34(7), 6628–6638, 2019. <https://doi.org/10.1109/TPEL.2018.2834304>.
- [12] F. Wang, H. Xie, Q. Chen, S. A. Davari, J. Rodriguez, and R. Kennel, 'Parallel Predictive Torque Control for Induction Machines Without Weighting Factors', *IEEE Trans. Power Electron.*, 35(2), 1779–1788, 2020. <https://doi.org/10.1109/TPEL.2019.2922312>.
- [13] J. Wang, F. Wang, Z. Zhang, S. Li, and J. Rodriguez, 'Design and Implementation of Disturbance Compensation-Based Enhanced Robust Finite Control Set Predictive Torque Control for Induction Motor Systems', *IEEE Trans. Ind. Inform.*, 13(5), 2645–2656, 2017. <https://doi.org/10.1109/TII.2017.2679283>.
- [14] S. A. Bednarz and M. Dybkowski, 'Estimation of the Induction Motor Stator and Rotor Resistance Using Active and Reactive Power Based Model Reference Adaptive System Estimator', *Appl. Sci.*, 9(23), 5145, 2019. <https://doi.org/10.3390/app9235145>.
- [15] I. Vicente, A. Endeman, X. Garin, and M. Brown, 'Comparative study of stabilising methods for adaptive speed sensorless full-order observers with stator resistance estimation', *IET Control Theory Appl.*, 4(6), 993–1004, 2010. <https://doi.org/10.1049/iet-cta.2008.0506>.
- [16] Y. Zhang, Z. Yin, Y. Zhang, J. Liu, and X. Tong, 'A Novel Sliding Mode Observer With Optimized Constant Rate Reaching Law for Sensorless Control of Induction Motor', *IEEE Trans. Ind. Electron.*, 67(7), 5867–5878, 2020. <https://doi.org/10.1109/TIE.2019.2942577>.
- [17] R. Yıldız, M. Barut, and E. Zerdali, 'A Comprehensive Comparison of Extended and Unscented Kalman Filters for Speed-Sensorless Control Applications of Induction Motors', *IEEE Trans. Ind. Inform.*, 16(10), 6423–6432, 2020. <https://doi.org/10.1109/TII.2020.2964876>.
- [18] C. Schauder, 'Adaptive speed identification for vector control of induction motors without rotational transducers', *IEEE Trans. Ind. Appl.*, 28(5), 1054–1061, 1992. <https://doi.org/10.1109/28.158829>.
- [19] V. Vasic, S. N. Vukosavic, and E. Levi, 'A stator resistance estimation scheme for speed sensorless rotor

- flux oriented induction motor drives', *IEEE Trans. Energy Convers.*, 18(4), 476–483, 2003. <https://doi.org/10.1109/TEC.2003.816595>.
- [20] M. N. Gayathri, S. Himavathi, and R. Sankaran, Performance enhancement of vector controlled drive with rotor flux based MRAS rotor resistance estimator. International Conference on Computer Communication and Informatics (ICCCI -2012), pp. 1–6, Coimbatore, India, 2012.
- [21] F. L. Mapelli, D. Tarsitano, and F. Cheli, 'MRAS rotor resistance estimators for EV vector controlled induction motor traction drive: Analysis and experimental results', *Electr. Power Syst. Res.*, 146, 298–307, 2017. <https://doi.org/10.1016/j.epsr.2017.02.005>.
- [22] R. Demir and M. Barut, 'Novel hybrid estimator based on model reference adaptive system and extended Kalman filter for speed-sensorless induction motor control', *Trans. Inst. Meas. Control*, 40(13), 3884–3898, 2018. <https://doi.org/10.1177/0142331217734631>.
- [23] A. V. R. Teja, C. Chakraborty, S. Maiti, and Y. Hori, 'A New Model Reference Adaptive Controller for Four Quadrant Vector Controlled Induction Motor Drives', *IEEE Trans. Ind. Electron.*, 59(10), 3757–3767, 2012. <https://doi.org/10.1109/TIE.2011.2164769>.
- [24] S. Basak, A. V. Ravi Teja, C. Chakraborty, and Y. Hori, A new model reference adaptive formulation to estimate stator resistance in field oriented induction motor drive. *39th Annual Conference of the IEEE Industrial Electronics Society (IECON 2013)*, pp. 8470–8475, Vienna, Austria, 2013.
- [25] T. Orłowska-Kowalska and M. Dybkowski, 'Stator-Current-Based MRAS Estimator for a Wide Range Speed-Sensorless Induction-Motor Drive', *IEEE Trans. Ind. Electron.*, 57(4), 1296–1308, 2010. <https://doi.org/10.1109/TIE.2009.2031134>.
- [26] M. Barut, S. Bogosyan, and M. Gokasan, 'Speed-Sensorless Estimation for Induction Motors Using Extended Kalman Filters', *IEEE Trans. Ind. Electron.*, 54(1), 272–280, 2007. <https://doi.org/10.1109/TIE.2006.885123>.
- [27] S. Haykin, Adaptive filter theory (3rd ed.). Prentice-Hall, Inc., Upper Saddle River, NJ, USA, 1996.
- [28] R. Yıldız, R. Demir, and M. Barut, Speed-sensorless predictive torque control of IM based on the adaptive fading extended Kalman filter. IV. International Turkic World Congress on Science and Engineering, pp. 82–93. Niğde, Turkey, 2022.
- [29] M. Habibullah, D. D. C. Lu, D. Xiao, J. E. Fletcher, and M. F. Rahman, 'Predictive Torque Control of Induction Motor Sensorless Drive Fed by a 3L-NPC Inverter', *IEEE Trans. Ind. Inform.*, 13(1), 60–70, 2017. <https://doi.org/10.1109/TII.2016.2603922>.

